Convention Special Issue – 2020

J. Indian Chem. Soc.,
Vol. 97, No. 12a, December 2020, pp. 2525-2532

Design of nanostructured materials for photocatalysis and photoelectrochemical applications†

Ashok K. Ganguli*[a], Anirban Das[b], Saikumar Manchala[a] and Shalini Tiwari[a]

[a]Department of Chemistry, Indian Institute of Technology Delhi, Hauz Khas, New Delhi-110 016, India

[b]Department of Chemistry, Biochemistry and Forensic Science, Amity School of Applied Sciences, Amity University Haryana, Manesar-122 413, Haryana, India

E-mail: ashok@chemistry.iitd.ac.in

Manuscript received online 12 November 2020, revised and accepted 27 December 2020

Utilization of abundant sunlight for a more sustainable future of our planet is a key endeavor of the scientific community. One of the major requirements for achieving this is the development of catalysts that are able to utilize light for chemical or Photo(electro)chemical transformations. Broadly these catalysts are composed either of semiconducting materials or materials that exhibit the surface plasmon resonance phenomenon. Nanostructured catalysts based on these materials are an important class of materials as their activity and selectivity can be tailored by variation of characteristics like size, morphology and aspect ratio. Our group has been very active for the last two decades in the development of nano-photocatalysts and nano-photoelectrocatalysts with controlled characteristics. We have utilized these materials for photodegradation of organic pollutants and photoelectrochemical splitting of water for production of clean fuels. This review presents a summary of the work carried out in our laboratory on development of photocatalysts and photoelectrocatalysts. The current state of art and our perspective of these fields is also provided.

Keywords: Photocatalysis, photoelectrocatalysis, nanostructured materials, water splitting.

1. Introduction

Investigation of properties of materials that possess photocatalytic properties as well as the processes that are involved in harvesting of light energy to achieve chemical and electrochemical transformations are of utmost importance for the development solar energy harvesting systems primarily for environmental remediation by reducing mankind's dependence on fossil fuels. Nanomaterials are attractive class of materials whose properties may be tuned by engineering their shape, size morphology, aspect ratio and such physical properties. These materials may also be combined with other materials to form composites and core-shell type materials[1] that give rise to unique properties. One of the major aims of development of composites and core-shell architectures is to increase the lifetime of the photo-generated excitons by effective separation of the electrons and the holes. Other aims of development of such structures include increase in the light absorption range of materials and passivation of surface defects on these materials that may result in exciton recombination. Tuning of surface facets by variation in phase of nanomaterials is another-technique that is used to tailor the photocatalytic activity of nano catalysts.

Our group has been active in development of novel nano photocatalysts as well as nano photo-electrocatalysts of varying physical characteristics[2]. Apart from synthesis and characterization of these materials, we have carried out extensive investigation of the photo and well as photo(electro) catalytic activity of these catalysts. Additionally, extensive mechanistic investigations have been carried out[3]. This mini-review summarizes the work done in our lab towards the development and evaluation of novel nanomaterials that have photo-catalytic and photo-electrocatalytic properties.

2. Nanostructured-photocatalysts

2.1. Oxide based semiconducting photocatalysts:

Semiconducting oxides are an important class of materials that have been reported as photocatalysts and photoelectrocatalysts. The primary advantage of these ma-

†Professor J. N. Mukherjee Memorial Lecture (2019).

terials is that they are cheap and synthetically easy to produce. Our group has reported numerous oxide materials with tailored photocatalytic properties. Spindle-shaped mesoporous TiO_2 nanostructures with a diameter of 6 nm and length of 30 nm were obtained by a simple based microemulsion route carried out at room temperature[4]. Apart from high thermostability, these nanospindles had a high surface area (200 $m^2 g^{-1}$) and were highly monodisperse. The photocatalytic efficiency was recorded to be about twice that of commercial TiO_2 and was comparable to the state of art titania-based photocatalyst (TiO_2 doped Pt) at the time of that report. The catalyst retained its efficiency even after three cycles.

Under alkaline conditions and an appropriate temperature, a template-free hydrothermal method resulted in nanocubes of cadmium tantalate and cadmium niobate with average edge-length of 15 nm[5]. The photocatalytic activity of these nanostructures was evaluated by degradation of Rhodamine B. The activating of the catalyst obtained by the low temperature methods (~600°C) is significantly (about seven times) enhanced as compared to that bulk oxides of the same composition obtained at higher temperatures (1000°C) by the solid state method. It was observed that nanoparticles obtained on hydrothermal treatment of 48 h exhibit the highest photocatalytic efficiency. The high efficiency was attributed to the high surface area of 57 $m^2 g^{-1}$ and enhanced adsorption of the cationic dye due to the highly negative surface charge. The nanoparticles are reasonably photostable.

Cu_2O NP of average size 25 nm were synthesized under an inert Ar atmosphere, at a low temperature of 350°C, with CuO (107 nm) and copper oxalate nanorods as precursors[6]. It was observed that in the absence of the oxalate nanorods also Cu_2O is obtained however a much higher temperature (850°C) is needed for the reaction. Additionally, the low temperature synthesis results in smaller particles of Cu_2O than the synthesis at higher temperatures. However, the Cu_2O synthesized at higher temperature is much more efficient (98%) in the degradation of methylene blue (MB) as compared to the low temperature sample that shows only 40% degradation.

Surface functionalized nanorods of the wide bandgap ZnO were synthesized[7] and evaluated for RhB decomposition. Two urea based imidazole compounds (R and S) were synthesized and these served as structure directing agents for the surface functionalized ZnO nanorods that were prepared using a low temperature (30–40°C) chemical precipitation route. Two varieties of R functionalized nanorods (R1 and R2) were prepared by using R: $Zn(NO_3)_2 \cdot 6H_2O$: NaOH in two ratios 1:2:4 and 1:1:1. For the S functionalized nanorods only one variety was prepared with the ratio of S: $Zn(NO_3)_2 \cdot 6H_2O$: NaOH being 1:2:4. The photocatalytic performance of R^1 was better than that of S1 in terms of percent degradation (84% vs 63%) under UV lamp irradiation for 3 h.

Spinel based $ZnMn_2O_4$ nanoparticles were obtained from the decomposition of metal oxalate precursors synthesized by the reverse micellar and the coprecipitation methods[8]. The method of synthesis was found to affect the shape, size and morphology of the oxalate precursors and oxides obtained from them. The reverse micellar method lead to micron-sized rod-shaped oxalate precursors whereas spherical nanoparticles of size 40–50 nm were obtained by the co-precipitation method. Treatment of these precursors at ~450°C yielded $ZnMn_2O_4$ nanoparticles. The particles obtained by co-precipitation were larger (40–50 nm) as compared to those obtained by the reverse micellar method (20–30 nm). Decomposition of methyl orange under UV-light irradiation was used as a test to evaluate photocatalytic activity.

The self-assembly of Pt NP on the surface of titania support by the photodeposition method was followed by TEM as a function of pH[9]. As model reactions, photocatalytic degradation of organic pollutants triclopyr and methyl orange were carried out using these bimetallic (Pt/TiO_2) catalysts. It was observed that the pH of the solution influenced the ionization state of the support which in turn affected the photodeposition and distribution of the Pt NP on the surface of TiO_2. The difference in photocatalytic activity was attributed to a mechanism based on differences in the inter particle interaction between the TiO_2 and the hydrolytic products of the metal ions.

Photocatalytic application of silica-supported tantalum oxide (ST) hollow spheres were evaluated in the UV range

(4.1 to 4.8 eV)[10]. The diameter of these nanostructures varied from 100–250 nm while the shell thickness varied from 24–58 nm.Tantalum isopropoxide and tetraethyl ortho silicate were hydrothermally treated at 120°C for 48 h in the presence of the capping agent, cetyl trimethyl ammonium bromide. A high surface area of 610 m^2 g^{-1} and pore size distribution variation from 13.4 to 19.0 nm was observed. The photocatalytic properties of these hollow spheres were found to be dependent of the Lewis acidity of silica and the contact area between SiO_2 and Ta_2O_5. As compared to pure Ta_2O_5, a 6-fold enhancement was seen in the photocatalytic activity of the silica-supported tantalum oxide hollow spheres. A simple, cheap but highly efficient technique for the fabrication of polydimethylsiloxane (PDMS) and polymethyl methacrylate (PMMA) based microfluidic microreactors was reported[11]. Spherical Ag_3PO_4 nanoparticles were synthesized using these microfluidic reactors and their photocatalytic activity was evaluated using decomposition of Rhodamine B under visible light irradiation as a model reaction. Within just 15 min, 97% degradation of the dye was observed.

2.2. Composite materials:

Engineering the bandgap of semiconductors by formation of composites and core-shell structures offers an excellent route to tune the optical and electronic properties of these semiconductor materials and thus aids in the development of more efficient photocatalysts. The formation of core-shell structures results in increased light harvesting capability as compared to individual photocatalysts. Additionally, such structures result in increased lifetime of the photogenerated excitons (electron-hole pairs) and result in increased photocatalytic efficiency. CuS nanostructures were decorated on the surface of ZnO nanotubes using a low-temperature wet-chemical method to form type-II semiconductors with p-n heterojunctions[12]. Initially CuO nanostructures were synthesized on the surface of ZnO nanotubes and then the CuO particles were converted to CuS at 80°C to generate these ZnO/CuS composite nanostructures. The decomposition of methylene blue under visible light irradiation was carried out to evaluate the photocatalytic efficiency of these nanostructures. Fig. 1(a) shows the TEM image of the ZnO/CuO core-shell nanorods while (b) presents a comparison of the photocatalytic activity of the different catalysts. Mechanistic investigations suggested that enhanced photocatalytic efficiency was due to efficient charge carrier separation due to formation of these heterojunctions.

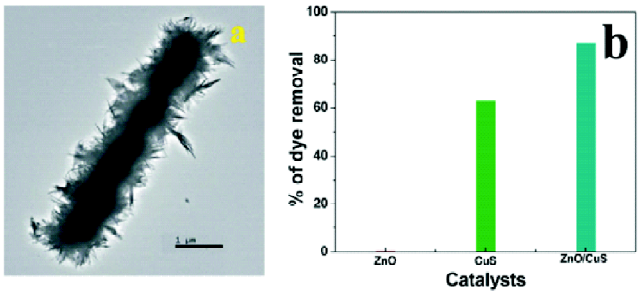

Fig. 1. (a) TEM image of the ZnO/CuO heterostructures in low magnifications and (b) bar diagram of % dye removal efficiency of bare ZnO, bare CuS and ZnO/CuS. Reproduced from *J. Mater. Chem. A*, 2014, **2(20)**, 7517 with permission from the Royal Society of Chemistry.

The photocatalytic properties of core-shell ZnO/CdS nanorod arrays were evaluated as a function of variation of shell thickness[13]. The average core diameter was 100 nm while the shell thickness was varied between 10 to 30 nm, by varying the concentration of citric acid added. Analysis of XRD data indicates that a compressive strain is obtained for core/shell nanorods while a tensile strain is obtained for ZnO nanorods. With growth of the shell, the band edge of the uncoated ZnO experiences a red shift in the UV-Visible spectra. Additionally, with the increase in shell thickness, a red shift in the emission band is seen in the steady-state photoluminescence (PL) spectra of the core/shell nanorod arrays. The separation of the photogenerated electron hole pairs in the ZnO/CdS core-shell arrays lead to a greater average lifetime of the core-shell structures as compared to the uncoated ZnO nanorods. The photocatalytic efficiency, as indicated by the photodegradation of Rhodamine B under simulated solar radiation, is also enhanced for the core-shell structures. The samples with shell thickness of 30 nm displayed the highest photocatalytic efficiency. In the I-V studies too, the samples with shell thickness of 30 nm exhibited a 16-fold current enhancement as compared to the bare ZnO nanorods.

ZnO/In_2S_3 core/shell nanorod arrays were synthesized to overcome the problem of electron hole recombination as

well as broaden the photo-response rate[14]. ZnO nanorods were surface functionalized using citric acid and In_2S_3 NP were grown on them. This resulted in increase in photocatalytic efficiency of decomposition of Rhodamine B using visible light with In_2S_3, ZnO nanorods and ZnO/In_2S_3 core/shell nanorod arrays exhibiting 35.0%, 2.7% and 83.7% degradation respectively. Additionally, a 6-fold enhancement (as compared to the dark current) was seen in the photoconductivity studies of core/shell nanorod arrays.

Ag_2S was also decorated on the surface of ZnO nanorods to produce bandgap engineered Ag_2S/ZnO core-shell structures[15]. To evaluate the performance of Ag_2S/ZnO core-shell structures in comparison to toxic Cd-based catalysts of similar architecture, ZnO/CdS core/shell nanostructures with the same thickness of the shell, were synthesized. The photocatalytic activity as indicated by the degradation of methylene blue confirmed that the degradation constant increased 40- and 2-times as compared to the pure ZnO and ZnO/CdS core/shell nanostructures, respectively. Apart from the more efficient light harvesting due to Ag_2S, the increased photocatalytic efficiency was also attributed to more efficient charge separation due to smaller conduction band offset between ZnO and Ag_2S. EPR spectroscopy was utilized to investigate the mechanism of the photodegradation process and the active species such as electrons, holes, hydroxyl radicals ($OH^{\bullet}$), and superoxide radical anions ($O_2^{\bullet-}$) were analyzed. It was determined that the hydroxyl radicals play a major role in the MB oxidation.

To compare the photocatalytic activity of core-shell structures as compared to composites of the same composition, TiO_2/CuS core/shell and composite nanostructures were synthesized and their photocatalytic activity was evaluated[16]. Core-shell structures were synthesized using a surface-functionalizing agent 3-mercaptopropionic acid while composites were synthesized without its use. The decomposition of methylene blue under visible light irradiation indicated that the photocatalytic performance of core shell structures was higher (90%) as compared to the composite structures (58%). This was attributed to the increased interfacial contact between TiO_2 and CuS aiding the localization of the electrons in the core and the holes in the shell, resulting in longer exciton recombination times. Mechanistic investigations via intermediate species analysis using mass spectrometry was carried out and it was determined that the demethylation pathway initiates the dye degradation.

$NaNbO_3$/CdS type-II core/shell heterostructures were also prepared by the aid of a surface functionalizing agent, 3-mercaptopropionic acid (MPA) and the degradation of methylene blue under visible light irradiation was investigated (Fig. 2)[17]. Compared to individual counterparts and Degussa P25, the photocatalytic standard, the resulting core/shell heterostructures had higher surface areas, enhanced light harvesting, and appreciably increased photocatalytic activity (Fig. 2b). The enhanced photocatalytic activity of these core/shell heterostructures was attributed to the efficient charge separation due to core/shell morphology and resulting type-II band alignment between $NaNbO_3$ and CdS (Fig. 2c). This band alignment aids the localization of one of the carriers in the core and the other in the shell. Active species scavenger studies were carried out to investigate the mechanism and it was determined that hydroxyl radicals ($OH^{\bullet}$) play an important role in the degradation mechanism.

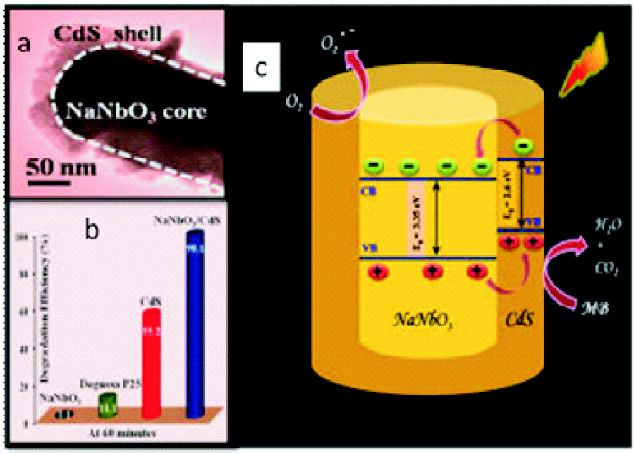

Fig. 2. TEM image of $NaNbO_3$/CdS core/shell heterostructures, degradation efficiency of $NaNbO_3$ nanorods, CdS nanoparticles, Degussa P25, and $NaNbO_3$/CdS core/shell heterostructures for the degradation of MB solution under visible light irradiation and Schematic diagram showing separation of photogenerated charge carriers in $NaNbO_3$/CdS core/shell heterostructures. Reprinted with permission from *ACS Appl. Mater. Interfaces,* 2014, **6(15)**, 13221. Copyright 2014 American Chemical Society.

2-Dimensional materials contribute to unique properties seen in composite materials. Supraparticles of size ~400 nm

comprising of 3–5 nm CdS quantum dots were synthesized, conjugated to graphene sheets and their photophysical properties and exciton dynamics were investigated[18]. Ultrafast electron transfer (<150 fs) from the CdS supraparticles to the graphene support was observed. Quenching of the CdS emission also supported this electron transfer. Enhanced stability of the exciton and more effective charge separation was observed in the composite as compared to the bare CdS supraparticles via ultrafast transient absorption spectroscopy. Photocatalytic degradation results indicate a five-fold enhancement in the rate when catalyzed by the composite as compared to when catalyzed by the bare CdS supraparticles.

An Ag_3PO_4 (20 nm) – mesoporus SiO_2 (200 nm) composite was evaluated as a visible light photocatalyst and a 52 times enhancement in rate of decomposition of RhB was observed in the composite as compared to the bare silver phosphate[19]. A charge carrier lifetime enhancement (~4 times as compared to the bare catalyst) was also observed in the composite. A composite contributes to reduction of per gram cost of the catalyst while resulting in higher photocatalytic activity. We also reported the photocatalytic activity of the nanocomposite g-C_3N_4-TiO_2 that was synthesized by a simple chemical route[20]. The composition with weight ratio 2:1 g-C_3N_4 to TiO_2 exhibits the maximum photocatalytic activity as quantified by photodegradation of Rhodamine B. This composition demonstrates an enhancement of 10 times over the activity of pure titania. The favorable band positions of the g-C_3N_4 and composite aid the charge separation and the increase in exciton lifetime leading to increased efficiency.

3. Nanostructured-photoelectrocatalysts

3.1. Semiconducting nanomaterials and their composites:

Photoelectrochemical experiments are a class of experiments that are used to evaluate catalysts that can convert light energy into electrical energy. We reported the synthesis of a TiO_2/CdS/Ag_2S core-shell shell (CSS) structure and evaluated its PEC performance[21]. As compared to pristine TiO_2 nanorods, PEC water splitting measurements using the CSS catalysts as photo-anodes yield low photocurrent onset potential of ~0.1 V and a high photocurrent density of ~7.6 mA/cm^2 at 1.0 V versus Ag/AgCl. Mott-Schottky analysis indicates that these heterostructures form a p-n junction that aids in effective separation of charges. The quenching of photoluminescence intensity and short average lifetime in CSS structures as evident from exciton dynamics study further support this observation. AgNi alloy nanoparticles were embedded in a graphitic carbon nitride (g-C_3N_4) polymer matrix by using an *in situ* solid-state heat treatment method to produce AgNi/g-C_3N_4 photocatalysts[22]. PEC activity evaluation indicated that this catalyst had the highest photocurrent density (1.2 mA cm^{-2}) reported for any doped g-C_3N_4 material. As a photocatalyst too, 95% degradation of RhB was achieved in 90 min.

Staggered gap core shell semiconductor $NaNbO_3$/Ag_2S heterostructures were synthesized, characterized and evaluated for PEC water splitting as well as for degradation of methylene blue[23]. A photocurrent density of 2.44 mA cm^{-2} at 0.9 V against Ag/AgCl reference electrode as well as a positive shift in onset potential by approximately 1.1 V was observed in a neutral Na_2SO_4 electrolyte. Efficient photoinduced interfacial charge transfer (IFCT) was postulated to be the reason for the high photoactivity.

We also reported the design and PEC as well as photocatalytic evaluation of catalysts in which specific facets were exposed to investigate the difference in activity[24]. It is known that variation in photocatalytic behavior is observed due to the variation in the surface energy of different facets. To elucidate the role of the different facets, $NaNbO_3$ was synthesized in the cubic and orthorhombic phases with crystals having cubic and cuboctahedron morphologies respectively. Thereafter $NaNbO_3$/CdS core-shell were prepared. The surface energies of the cubic phase comprising the 100 family of facets and the orthorhombic phase comprising the (110) and (114) facets of the $NaNbO_3$ were calculated and different mechanisms were proposed for photocatalytic activity based on these calculations. As theoretically predicted, experimentally too, it was seen that the cubic phase was catalytically more active than the orthorhombic phase.

To demonstrate the superiority of Z-scheme as compared to Type-II band alignment, $NaNbO_3$/$CuInS_2$/In_2S_3 (core/shell/shell) and $NaNbO_3$/In_2S_3/$CuInS_2$ (core/shell/shell) were synthesized (Fig. 3)[25]. The former has a Z-scheme (Fig. 3d)

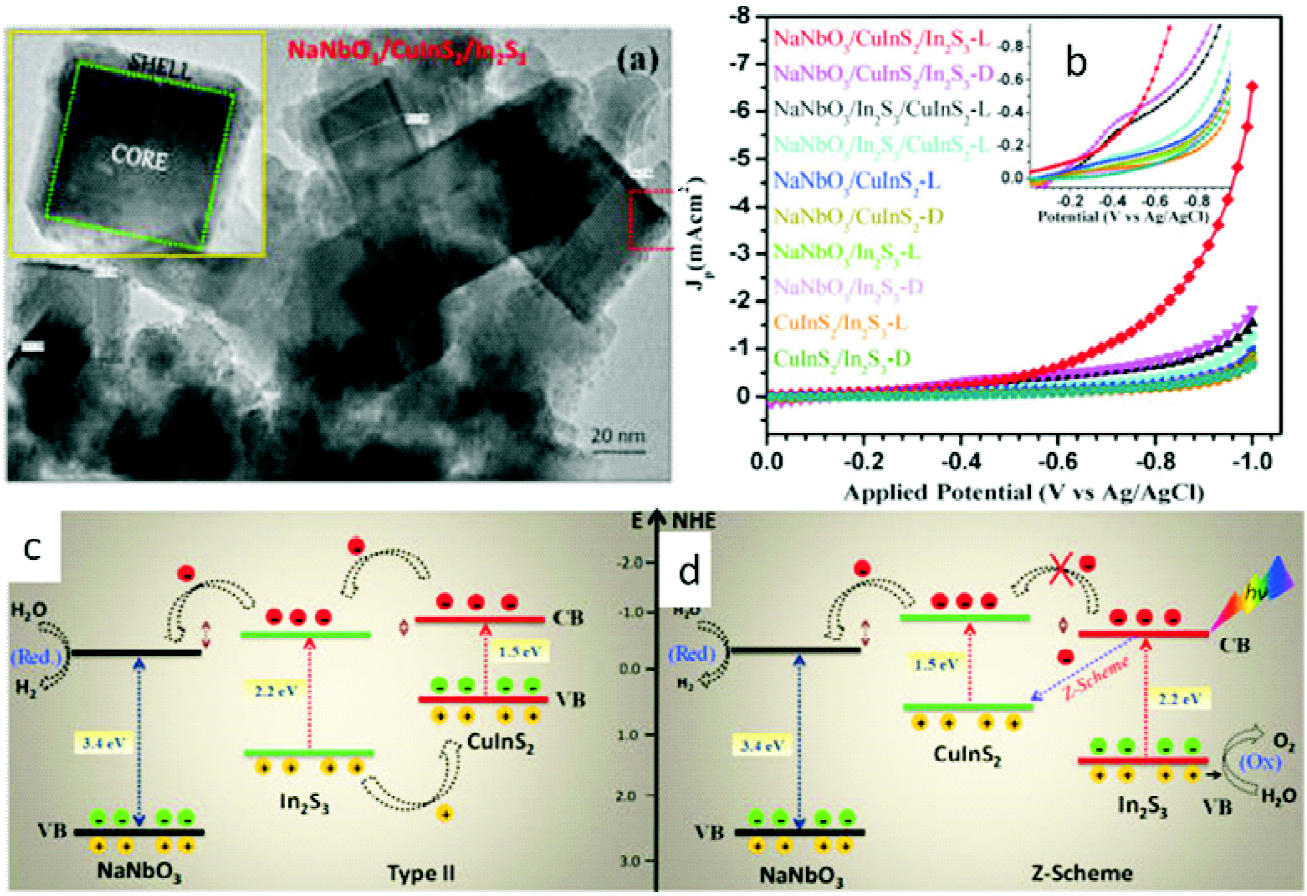

Fig. 3. (a) TEM image of Z-scheme $NaNbO_3/CuInS_2/In_2S_3$ core/shell heterostructures, photoelectrochemical measurement of synthesized core/shell heterostructures (inset: the magnified photocurrent density) and schematic representation of (a) Type-II and (b) Z-Scheme band alignment between $NaNbO_3/In_2S_3/CuInS_2$ and $NaNbO_3/CuInS_2/In_2S_3$ core/shell heterostructures respectively. Reprinted with permission from *Inorg. Chem.,* 2018, **57(24)**, 15112. Copyright 2018 American Chemical Society.

while the latter has a Type-II band alignment (Fig. 3c). Photoelectrochemical (PEC) water splitting studies and as well as photocatalytic degradation of organic pollutants confirm that the structure with Z-scheme has a higher current density and a lower onset potential as compared to the structures with Type-II alignment (Fig. 3b).

3.2. Plasmonic nanomaterials:

Apart from other semiconductors, we also investigated PEC activity of SPR active nobel metals used to sensitize semiconductors. Photocorrosion resistant Au nanoparticles (NPs) (< 5 nm in size) in very low concentration (0.5–1 wt%) were decorated on the surface of P25-titania to extend its photocatalytic activity to the visible region (Fig. 4)[26]. These Au-P25-TiO_2 nanocomposites with varying concentration of Au NP (loading of 0.5, 0.6, 0.7, 0.8 and 1 wt% labelled as samples PA1 to PA5 respectively) were synthesized and characterized. P25C refers to unloaded P25-TiO_2, calcined in under the same conditions. The PEC response indicates that at lower Au loadings the photocurrent increases with Au concentration to maximize at a loading of 0.7 wt% Au, but subsequently at higher loadings the photocurrent decreases monotonically (Fig. 4a). This behavior was attributed to a balance between charge carrier density (Nd, a kinetic parameter) and the flatband potential (VFB, a thermodynamic parameter) as indicated by the Mott-Schottky analysis (Fig. 4c and d).

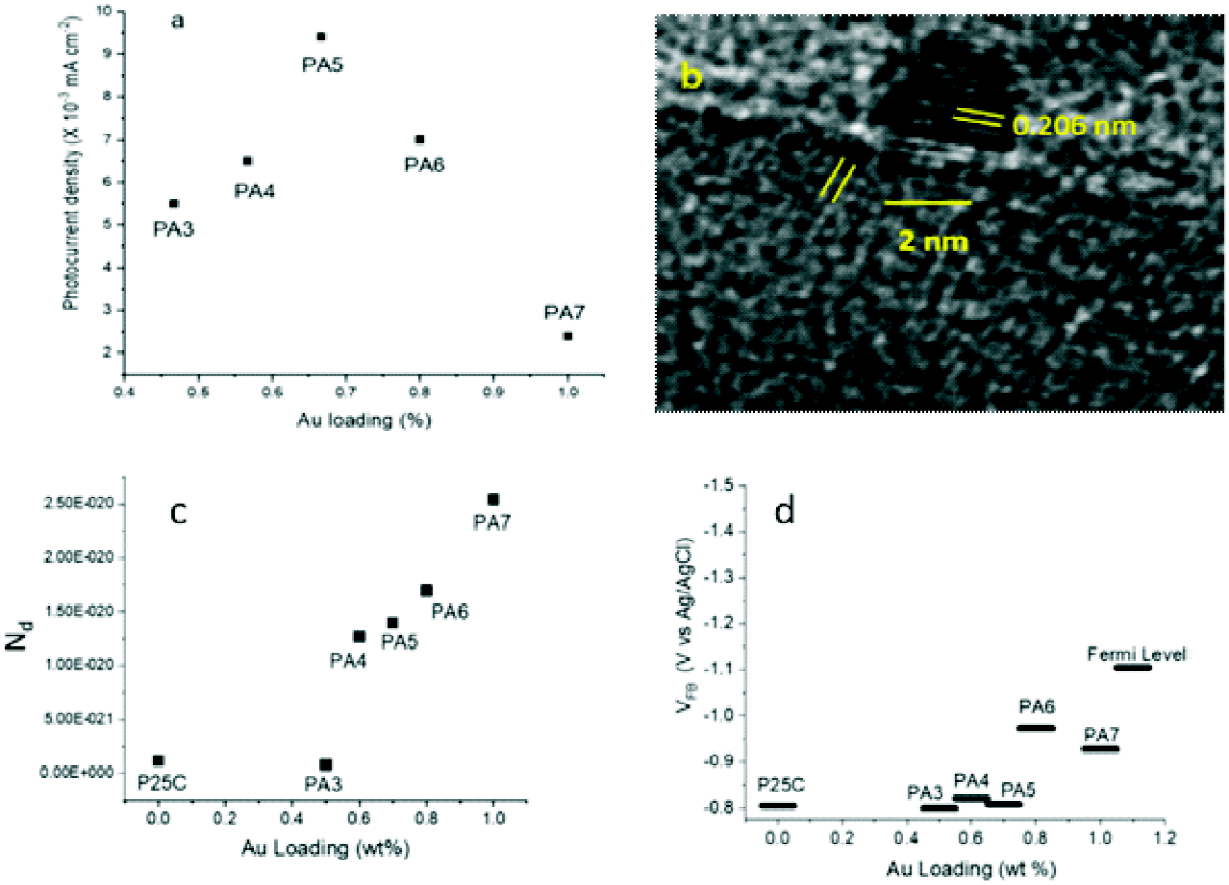

Fig. 4. (a) Variation of photocurrent as a function of Au loadings, (b) HRTEM image of Au-P25-TiO_2 nanocomposite, (c) charge carrier density (Nd) and (d) flatband potential (V_{FB}) trends for P25C, PA3, PA4, PA5, PA6 and PA7. Reprinted from A. Das, P. Dagar, S. Kumar and A. K. Ganguli, Effect of Au nanoparticle loading on the photo-electrochemical response of Au-P25-TiO_2 catalysts. *Journal of Solid State Chemistry,* 2020, **281**, 121051, with permission from Elsevier.

4. Conclusions and perspectives

In summary, we have reported a variety of compositions, and physical characteristics namely shape, structure and morphology of nanomaterials, that were used as efficient photocatalysts and photo(electro)catalysts. Our initial efforts were directed to the development of individual semiconductor materials, primarily semiconducting oxides. Variation of the physical characteristics was seen to effect the photocatalytic performance of these nanostructures. Thereafter, primarily to increase the exciton lifetime and thus result in higher efficiency, composites and nanostructures with specialized geometry like core-shell structure were synthesized and evaluated for photocatalysis. Indeed, it was observed that the performance of these composites and core-shell structures was better (in some cases by an order of magnitude) than the individual semiconductors. Additionally, we reported enhancement in photocatalytic and photo-(electro)catalytic performance by variation of the surface facets in these structures achieved by variation of the phases. We also reported core-shell-shell type structures and engineered the synthesis to produce both Type-II and z-scheme band alignment. It was seen that, as expected, the latter exhibited better photocatalytic and photo(electro)catalytic performance than the former.

Though, much progress has been made in the development of photo and photo(electro)catalysts still commercial utilization of the novel nanomaterials with exotic architecture has still not been achieved. Still, silicon based solar cells are

cheaper to produce and have a higher photcatalytic efficiency than the nanomaterials being developed worldwide. One of the fields where more effort needs to be directed is theoretical studies of these nanomaterials, a field which is yet to mature fully. This would aid in more directed experimental research endeavors that would be based on sound theoretical groundwork. Another, area to direct resources is techniques to synthesize nanomaterials on a commercial scale. Most of the research carried out is on a laboratory scale and this prevents commercial utilization of the materials produced, primarily due to the higher cost associated with small scale production.

References

1. A. K. Ganguli, A. Das and K. Natarajan, *The Chemical Record,* 2020, **20(5)**, 371.
2. A. Ganguly, O. Anjaneyulu, K. Ojha and A. K. Ganguli, *CrystEngComm.,* 2015, **17(47)**, 8978.
3. S. Kumar, K. Ojha and A. K. Ganguli, *Adv. Mater. Interfaces,* 2017, **4 (7)**, n/a.
4. D. Das, A. Shivhare, S. Saha and A. K. Ganguli, *Mater. Res. Bull.,* 2012, **47(11)**, 3780.
5. D. Das and A. K. Ganguli, *RSC Adv.*, 2013, **3(44)**, 21697.
6. B. Kumar, S. Saha, A. Ganguly and A. K. Ganguli, *RSC Adv.,* 2014, **4(23)**, 12043.
7. J. Mishra, M. Jha, N. Kaur and A. K. Ganguli, *Mater. Res. Bull.,* 2018, **102**, 311.
8. M. Mohammed Qamar, S. E. Lofland, K. V. Ramanujachary and A. K. Ganguli, *Bull. Mater. Sci.,* 2009, **32(3)**, 231.
9. M. Qamar and A. K. Ganguli, *Bull. Mater. Sci.,* 2013, **36(6)**, 945.
10. M. Sharma, D. Das, A. Baruah, A. Jain and A. K. Ganguli, *Langmuir,* 2014, **30(11)**, 3199.
11. A. Singh, A. Baruah, V. Katoch, K. Vaghasiya, B. Prakash and A. K. Ganguli, *J. Photochem. Photobiol. A,* 2018, **364**, 382.
12. M. Basu, N. Garg and A. K. Ganguli, *J. Mater. Chem. A,* 2014, **2(20)**, 7517.
13. S. Khanchandani, S. Kundu, A. Patra and A. K. Ganguli, *J. Phys. Chem. C,* 2012, **116(44)**, 23653.
14. S. Khanchandani, S. Kundu, A. Patra and A. K. Ganguli, *J. Phys. Chem. C,* 2013, **117(11)**, 5558.
15. S. Khanchandani, P. K. Srivastava, S. Kumar, S. Ghosh and A. K. Ganguli, *Inorg. Chem.,* 2014, **53(17)**, 8902.
16. S. Khanchandani, S. Kumar and A. K. Ganguli, *ACS Sustainable Chem. Eng.,* 2016, **4(3)**, 1487.
17. S. Kumar, S. Khanchandani, M. Thirumal and A. K. Ganguli, *ACS Appl. Mater. Interfaces,* 2014, **6(15)**, 13221.
18. K. Ojha, T. Debnath, P. Maity, M. Makkar, S. Nejati, K. V. Ramanujachary, P. K. Chowdhury, H. N. Ghosh and A. K. Ganguli, *J. Phys. Chem. C,* 2017, **121(12)**, 6581.
19. M. Sharma, K. Ojha, A. Ganguly and A. K. Ganguli, *New J. Chem.,* 2015, **39(12)**, 9242.
20. M. Sharma, S. Vaidya and A. K. Ganguli, *J. Photochem. Photobiol. A,* 2017, **335**, 287.
21. S. Kumar, A. P. Singh, N. Yadav, M. Thirumal, B. R. Mehta and A. K. Ganguli, *ChemistrySelect,* 2016, **1(15)**, 4891.
22. N. Bhandary, A. P. Singh, S. Kumar, P. P. Ingole, G. S. ThakurA. K. Ganguli and S. Basu, *ChemSusChem.,* 2016, **9(19)**, 2816.
23. S. Kumar, A. P. Singh, C. Bera, M. Thirumal, B. R. Mehta and A. K. Ganguli, *ChemSusChem.,* 2016, **9(14)**, 1850.
24. S. Kumar, R. Parthasarathy, A. P. Singh, B. Wickman, M. Thirumal and A. K. Ganguli, *Catal. Sci. Technol.,* 2017, **7(2)**, 481.
25. S. Kumar, N. Yadav, P. Kumar and A. K. Ganguli, *Inorg. Chem.,* 2018, **57(24**), 15112.
26. A. Das, P. Dagar, S. Kumar and A. K. Ganguli, *Journal of Solid State Chemistry,* 2020, **281**, 121051.